

Bayesian Inverse Ising Problem with Three-body Interactions

Godwin Osabutey^{*1}, Robert Richardson^{†2}, and Garritt L. Page^{‡2}

¹Department of Mathematics, University of Bologna, Bologna, Italy

²Department of Statistics, Brigham Young University, Provo, USA

April 9, 2024

Abstract

In this paper, we solve the inverse Ising problem with three-body interaction. Using the mean-field approximation, we find a tractable expansion of the normalizing constant. This facilitates estimation, which is known to be quite challenging for the Ising model. We then develop a novel hybrid MCMC algorithm that integrates Adaptive Metropolis Hastings (AMH), Hamiltonian Monte Carlo (HMC), and the Manifold-Adjusted Langevin Algorithm (MALA), which converges quickly and mixes well. We demonstrate the robustness of our algorithm using data simulated with a structure under which parameter estimation is known to be challenging, such as in the presence of a phase transition and at the critical point of the system.

Key words: Higher-order interaction, intractable likelihood, mean-field model, phase transition

1 Introduction

Graphical models have proven to be valuable tools for modeling network data, effectively capturing the interactions between agents/units or nodes. Gaining insights into these intricate networks of interactions holds far-reaching significance across various domains, including social sciences (McFadden, 2001; Durlauf, 1999; Brock and Durlauf, 2001; Contucci and Vernia,

*godwin.osabutey2@unibo.it

†richardson@stat.byu.edu

‡page@stat.byu.edu

2020; Barra et al., 2014; Gallo et al., 2009), structural biology (Schug et al., 2009; Morcos et al., 2011), neuroscience (Schneidman et al., 2006; Mézard and Mora, 2009), marketing (Bury, 2013), finance (Borysov et al., 2015), psychometric networks (Burger et al., 2022; Marsman and Rhemtulla, 2022), socio-economic sciences and others (Opoku et al., 2019; Geman and Graffigne, 1986; Burioni et al., 2015; Osabutey et al., 2020). The estimation of these interactions involves solving an inverse problem, specifically, estimating the network parameters from observed data. In the inverse problem, observations of the system are made through experimentation or measurement, with the aim of drawing conclusions about the system based on its microscopic interactions. This involves calculating interactions and biases between agents using statistical summaries of the macroscopic variables. In statistical terms, macroscopic variables are related to the mean (or some other summary), while microscopic aspects often deal with individual data points.

In this paper, we use the Bayesian paradigm to address an inverse problem for a class of statistical mechanics mean-field models. Specifically, we focus on the Ising mean-field model, introduced in Contucci et al. (2022, 2023, 2024), which incorporates both three-body and two-body interactions, along with a bias or external field. Network models conventionally are built solely on two-body interactions, but recent advances have introduced higher-order interactions, which allows for a more complex and rich network structure. That said, the added flexibility makes analytical solutions and parameter estimation more difficult. In Contucci et al. (2023), the inverse Ising problem with three-body interaction was solved using the method of moments (i.e., naïve mean-field method). However, a key drawback of their approach we aim to solve using a Bayesian methodology is the inability to accommodate critical points (i.e., points where the system begins to transition) nor estimate parameters in the presence of phase transition unless said transition is known to exist *a priori*. Phase transition typically results in a multimodal density, which requires a two- or more-step procedure in traditional statistical physics approaches (Contucci et al., 2023). Our Bayesian

approach is able to very easily ameliorate this drawback.

The Bayesian approach that we adopt is also more practical than approaches commonly employed in statistical physics. In traditional approaches, even simple modifications of the model (i.e., moving from two- to three-body interactions) can be cumbersome as they would require analytically solving a new inverse problem, which may not even be possible. Our Bayesian approach is much more easily able to accommodate model modifications via MCMC sampling.

A complication that arises when considering Bayesian Ising models is the intractability of the normalizing constant which makes MCMC sampling quite challenging. Due to this, various approximation techniques have been proposed in the literature to tackle the intractability of the normalizing constant in Bayesian inverse problems. For instance, a recent study (Kim et al., 2021) introduced a variational Bayes approach, utilizing a pseudo-likelihood to approximate the true likelihood. Habeck (2014) proposed reweighing techniques to approximate the normalization constant and employed a sequential Monte Carlo algorithm for posterior sampling. With all that said, an additional contribution we make is to show that under the assumption of a fully connected graph, the normalizing constant is analytically tractable which makes MCMC computation feasible. Thus, we leverage mean-field theory to simplify the network structure which permits calculating the normalizing constant. While the mean-field assumption simplifies the network structure, it still provides an analytically viable setting and a fair description of phase separation in dimensions $d \geq 4$ (Weiss, 1907; Baxter, 2016).

Even though our approach makes it possible to calculate the normalizing constant, commonly used MCMC algorithms still exhibit slow convergence and poor mixing. Thus, a final contribution we make is the development of novel MCMC strategies for the Ising model based on Adaptive Metropolis Hastings (AMH), Hamiltonian Monte Carlo (HMC), and the Manifold-Adjusted Langevin Algorithm (MALA) that result in chains that mix well and

converge quickly.

Our approach to studying the method we propose is to illustrate its performance in scenarios where estimating a three-body interaction by way of an Ising model is notoriously difficult. This is done by simulating realizations of the system for some fixed model parameters and then using our approach to accurately estimate or recover the model parameters associated with certain macroscopic observables. The rest of the paper is organised as follows: Section 2 provides more context to the model and constructs a method for analyzing the likelihood, Section 3 discusses how to build a Bayesian model and develops an algorithm to draw samples from the posterior distribution of model parameters, Section 4 details a number of scenarios that are considered challenging, and Section 5 contains a brief conclusion. All proofs of results for the expansion of the normalizing constant are provided in the Appendix A and Appendix B has some simulation results.

2 The model and methods

Before providing model details, we first provide context regarding the system we study. We consider an Ising model with a constant mean shift (i.e., bias) and isotropic two-body and three-body interactions. The Ising spins will denote agents or units and their orientation signifies their respective actions that can potentially be influenced by their neighbors. For instance, consider a system made-up of N interacting agents within a network. In this system, agents are positioned on the vertices, and their orientation signifies their respective actions. Actions may include, for example, to buy or sell stock at a given period, to vote in an election or not, in favor of death penalty or not, to travel by air or by land, neurons firing (spiking) or at rest etc.. Denote by x_i the i th vertex variable, distributed in $\{-1, 1\}$ and $\mathbf{x} = (x_i)_{i \leq N}$ a random vector denoting the action of all agents in the network, i.e., the state of the system which can be observed or measured. Our interest is to perform statistical

inference on the network by estimating the interactions between agents and biases. This endeavor has garnered significant attention in the natural and social sciences, leading to the development of various techniques to address it. These include the Bayesian approach (Kim et al., 2021; Habeck, 2014; Li and Zhang, 2010), maximum likelihood (Contucci et al., 2023; Chatterjee, 2007), naïve mean-field theory (nMF) (Contucci et al., 2023; Opoku et al., 2019; Burioni et al., 2015; Kappen and Rodríguez, 1998; Fedele et al., 2013; Decelle and Ricci-Tersenghi, 2016; Contucci et al., 2017; Nguyen et al., 2017), pseudolikelihood maximisation (PLM) (Chatterjee, 2007; Aurell and Ekeberg, 2012; Bhattacharya and Mukherjee, 2018), minimum probability flow learning (Sohl-Dickstein et al., 2011) and many others.

The network structure considered extends beyond the usual graph-theoretical setting of vertices and edges to a richer hypergraph environment where the three-body terms, representing faces, gain significance. Higher-order graphs involving three or more agents interaction has a significant impact on the dynamics of the system, leading to abrupt transitions between the states of the system (Battiston et al., 2021; Benson et al., 2018; Subramanian and Lebowitz, 1999). A novel feature of this model is the presence of first-order phase transition in the cubic interaction parameter (Contucci et al., 2024). These abrupt transitions, often referred to as the tipping point phenomenon in sociology, represent critical points that trigger substantial changes when crossed (Benson et al., 2018; Alvarez-Rodriguez et al., 2021). Such abrupt phase transitions, exemplified by phenomena like political revolutions (Goldstone, 2015; Skocpol, 1979), are of particular interest from a statistical standpoint due to their inherent complexity. Understanding, controlling, and predicting outcomes in networks experiencing abrupt transitions pose unique challenges compared to scenarios involving continuous transitions, such as cultural shifts (Hamilton et al., 2016; Inglehart, 2020). We next detail the mean-field Ising model.

2.1 The mean-field Ising model

Consider a system defined by the Ising model on an undirected graph with N agents on the vertices $x_i, i = 1, \dots, N$. Agents are assumed to be binary random variables with $x_i \in \{-1, 1\}$ and denote by $\mathbf{x} = (x_1, \dots, x_N) \in \{-1, 1\}^N$ the network configuration describing the state of the system. The joint distribution of x_i for a given state \mathbf{x} , is given by a Boltzmann-Gibbs type distribution:

$$P(\mathbf{x}; \boldsymbol{\theta}) = \frac{e^{-\beta H(\mathbf{x}; \boldsymbol{\theta})}}{Z}, \quad (1)$$

where $Z = \sum_{\mathbf{x} \in \{-1, 1\}^N} e^{-\beta H(\mathbf{x}; \boldsymbol{\theta})}$ is the normalisation constant, also known as the partition function, that turns $P(\mathbf{x}; \boldsymbol{\theta})$ into a probability measure, $H(\mathbf{x}; \boldsymbol{\theta})$ is the so called Hamiltonian with parameter vector $\boldsymbol{\theta}$, and β is the usual inverse temperature. In what follows we define the Hamiltonian as:

$$H(\mathbf{x}; \boldsymbol{\theta}) = - \sum_{\langle i, j, k \rangle} K_{ijk} x_i x_j x_k - \sum_{\langle i, j \rangle} J_{ij} x_i x_j - \sum_i h_i x_i, \quad (2)$$

so that $\boldsymbol{\theta} = (\{K_{ijk}\}, \{J_{ij}\}, \{h_i\})$. The first term of (2) modulates interaction between triples of vertex variables, the second term modulates interactions between pairs while the third term controls the effect of external field acting on each unit of the graph. K_{ijk} is the interaction strength between vertices i, j and k , J_{ij} is the strength of interaction between pairs of vertices i and j , and h_i is the external field parameter. If $K_{ijk} = 0$, then vertices i, j and k are not connected by edges while connected if $K_{ijk} \neq 0$. Likewise, whenever $J_{ij} = 0$, then vertices i and j are not connected by an edge.

As mentioned, we make the mean-field approximation (i.e., the graph representing the system is fully connected), implying that each vertex x_i is assumed to be independent and identically distributed (*iid*). In this way, the network configuration \mathbf{x} can be completely summarized through its mean. This leads to having isotropic couplings and fields by setting:

$K_{i,j,k} = K/3N^2$, $J_{i,j} = J/2N$ and $h_i = h$. As a result, the dimension of the parameter vector is reduced to $\boldsymbol{\theta} = (K, J, h) \in \mathbb{R}^3$. Here, $\boldsymbol{\theta}$ is fixed so that, K describes the interaction strength between all triples of vertex variables, J describes the strength of interaction between all pairs and h is the global external field of influence on all vertices. The factors $1/2N$ and $1/3N^2$ are the normalization of the couplings and eliminates the double and triple counting of interactions between pairs and triples of the vertex variables over the sum in (2), respectively. Therefore we can write the Hamiltonian (2) as:

$$H(\boldsymbol{x}; \boldsymbol{\theta}) = -N \left(\frac{K}{3} m_N^3(\boldsymbol{x}) + \frac{J}{2} m_N^2(\boldsymbol{x}) + h m_N(\boldsymbol{x}) \right), \quad (3)$$

where $m_N(\boldsymbol{x}) = \frac{1}{N} \sum_{i=1}^N x_i$ is the main observable of the system, i.e., the mean value of a given \boldsymbol{x} . Observe that (3) is a representation of (2) in its macroscopic state due to the introduction of $m_N(\boldsymbol{x})$ for a given configuration \boldsymbol{x} . A key advantage of the Ising model is its ability to explain the aggregate behavior of an interacting system. In this sense, to compute the likelihood for a given configuration \boldsymbol{x} with $m_N(\boldsymbol{x}) = m \in [-1, 1]$, requires computing the number of possible configurations that share the same mean value m . This is a consequence of the fact that different orientation of the x_i for $i = 1, \dots, N$ may produce the same macroscopic behavior (i.e. $m_N(\boldsymbol{x})$) and that $P(\boldsymbol{x}; \boldsymbol{\theta})$ assigns equal probability to such configurations.

The normalization constant Z in equation (1) lacks a closed form, necessitating a precise expansion. Several methods in the literature have been employed to expand Z , including the Gaussian (Hubbard-Stratonovich) transform, cell or cluster approximation, series expansion (Baxter, 2016), and large deviations techniques. In this study, we rely on large deviation methods, primarily due to the non-convex nature of the Hamiltonian (3), where the Gaussian transform is inefficient for providing an approximation. In this context, we draw on ideas from statistical mechanics, allowing the characterization of the microscopic behavior of a

physical system through its macroscopic properties. Subsequently, we assume that β in (1) is absorbed by $\boldsymbol{\theta}$.

Remark 2.1. *The normalizing constant Z can be written as:*

$$Z = \sum_{m \in S_m} A_N(m) e^{-H(\mathbf{x}; \boldsymbol{\theta})} \quad (4)$$

where $S_m = \{-1 + \frac{2k}{N}, k = 0, \dots, N\}$ is the spectrum of $m_N(\mathbf{x})$ and $A_N(m) = \text{card}\{\mathbf{x} \in \{-1, 1\}^N : m_N(\mathbf{x}) = m\}$ counts configurations of \mathbf{x} with the same $m_N(\mathbf{x})$ value.

According to Talagrand (2003) and Baxter (2016), we can compute bounds on $A_N(m)$ to derive a closed form of Z which can then be utilized to establish the existence of the thermodynamic limit of the free energy, describing the asymptotic properties of the system:

Lemma 2.1. *Let $\Omega = \{+1, -1\}^N$ denote the set of all possible configurations of the network. Then for $A_N(m) \in \mathbb{N}$ the following inequality holds:*

$$\frac{1}{L\sqrt{N}} e^{-NI(m)} \leq A_N(m) \leq e^{-NI(m)}$$

where L is a universal constant and,

$$I(m) = \frac{1-m}{2} \log\left(\frac{1-m}{2}\right) + \frac{1+m}{2} \log\left(\frac{1+m}{2}\right)$$

Proof. See Appendix A. □

Now, notice that the sum over 2^N vertex configurations becomes the sum over $(N+1)$ possible macrostates, i.e. $|S_m|$. Since A_N is the exact number of possible configurations that have the same macrostate $m_N(\mathbf{x}) = m$, we can express (1) as:

$$P(m_N(\mathbf{x}) = m) = \sum_{\mathbf{x} \in \Omega: m_N(\mathbf{x}) = m} \frac{e^{-H(\mathbf{x}; \boldsymbol{\theta})}}{Z} = \frac{A_N e^{-H(\mathbf{x}; \boldsymbol{\theta})}}{\sum_{m \in S_m} A_N e^{-H(\mathbf{x}; \boldsymbol{\theta})}}. \quad (5)$$

Therefore, to obtain the probability of the system being in a given state with $m_N(\mathbf{x}) = m$, we use the exact likelihood function defined by (5) contrary to the approximated version via pseudo-likelihood (Kim et al., 2021) since we are interested in the behavior on the average. In this work, we use the exact definition of A_N found in equation (7) of the Appendix. Observe that by substituting the bounds of A_N into (5), we will obtain a large deviation principle (LDP) for the sample mean $m_N(\mathbf{x})$.

We denote by $Eg(\mathbf{x})$ the expected value of an observable $g(\mathbf{x})$ with respect to the measure (5):

$$Eg(\mathbf{x}) = \sum_{\mathbf{x} \in \Omega: m_N(\mathbf{x})=m} g(\mathbf{x})P(m_N(\mathbf{x}) = m). \quad (6)$$

In the forward problem, the quantity of interest are the moments, i.e. the expected mean value for a given configuration $Em_N(\mathbf{x})$ and correlations. In this study, our primary objective is to determine the values of the parameters $\boldsymbol{\theta} = (K, J, h)$, assuming full knowledge of \mathbf{x} . This analysis is carried out under the assumption of full connectivity among the vertices.

Since we adopt a Bayesian approach, to finish the model specification based on (1) with Hamiltonian (3) it is required to specify a prior distribution for $\boldsymbol{\theta} = (K, J, h)$. We employed the following weakly informative priors $K \sim N(0, 2)$, $J \sim N(0, 2)$, $h \sim N(0, 2)$. We note however that our experiments are based on a large N making it so that prior specification has little influence on resulting inference. Note further that the Bayesian approach adopted here offers a more flexible and efficient estimation technique as opposed to the ones introduced in (Contucci et al., 2023; Kim et al., 2021). For instance, here, we do not need to compute the *free-energy* and study its derivatives to obtain analytical inverse formulas for the parameters as was done in Contucci et al. (2023) and we do not need to have access to individual data points to compute the likelihood function as in Kim et al. (2021).

2.2 Identifiability

We briefly mention in this section a peculiar property underlying the inverse problem machinery that leads to nonidentifiability in the parameter space. To our knowledge, the issue of nonidentifiable parameters in the inverse Ising problem with two- or three-body interactions has not been addressed in the existing literature. In the context of statistical physics, we define nonidentifiable parameters as sets of distinct parameter pairs or triples that yield nearly identical model predictions, such as magnetization, susceptibility, and higher-order moments. Magnetization and susceptibility denotes simply the sample mean and variance respectively. The limited information contained in the data and the nature of inferring parameters from that data can make it challenging to distinguish certain combinations of parameters.

The challenge of identifying model parameters from given data can arise due to various factors. These include insufficient or noisy data, invariance of the Hamiltonian under certain symmetries or transformations, and certain statistical properties of the model such as parameter trade-offs where MCMC sampling becomes infeasible (Raue et al., 2013). In these scenarios, the likelihood function may favor other optimal parameter values different from the original ones used for data generation as it explores the parameter space (Raue et al., 2009, 2013). We highlight this behavior in one of the parameter scenarios described in Section 4

3 Markov Chain Monte Carlo algorithm

The classical Metropolis Hastings sampling for this problem leads to bad mixing due to high correlations between variables. Hence, three advanced sampling algorithms were developed to mitigate the mixing and convergence issues. In particular, we considered adaptive Metropolis Hastings (AMH), Metropolis-adjusted Langevin algorithm (MALA), and Hamiltonian Monte

Carlo (HMC) algorithms. While all three improved the mixing, the most consistent method found was a combination of all three.

The AMH adjusts the covariance structure of the proposal distribution at each iteration of the algorithm using the sampled values at previous iterations. In many scenarios it can intelligently tune the algorithm to force good acceptance rates and therefore good mixing. However, for the Ising model with three-body interaction, the correlation between parameters is physically driven in such a way that acceptance rates were never able to get into acceptable ranges and mixing remained poor, especially when the starting values for the algorithm were not close to the truth. This will be illustrated in Section 4.

MALA attempts to use the geometry of the likelihood function to make proposals. In its standard form the proposal for new parameter values is $\boldsymbol{\theta}^* = \boldsymbol{\theta} + \varepsilon^2 \Delta \mathcal{L}(\boldsymbol{\theta})/2 + \varepsilon z$, where $\boldsymbol{\theta}$ denotes the parameter value to recover, ε is an integration step size, \mathcal{L} is the log-likelihood function of (5), and z is a standardised normal variable. Limit theorems have shown that when variables are correlated, using manifold geometry improves sampling. This involves a metric tensor G and proposals are made using $\boldsymbol{\theta}^* = \boldsymbol{\theta} + \varepsilon^2 G(\boldsymbol{\theta}) \Delta \mathcal{L}(\boldsymbol{\theta})/2 + \sqrt{G(\boldsymbol{\theta})} \varepsilon z$. Despite MALA using the geometry of the model parameter space to make more educated proposals, in the model considered here, it still resulted in low acceptance rates and bad mixing. Thus, we don't employ stand alone MALA, but rather use it to improve the performance of Hybrid algorithms that we now describe.

HMC introduces a series of normally distributed latent momentum parameters, $p \sim N(0, \mathbb{M})$, with covariance matrix \mathbb{M} representing a mass matrix. Proposals are made for both the model parameters and latent momentum parameters using a leapfrog procedure.

One leapfrog step of size ε can be made using

$$\begin{aligned}
 p(\tau + \varepsilon/2) &= p(\tau) + \varepsilon \Delta \mathcal{L}(\boldsymbol{\theta}(\tau))/2 \\
 \boldsymbol{\theta}(\tau + \varepsilon) &= \boldsymbol{\theta}(\tau) + \varepsilon \mathbb{M}^{-1} p(\tau + \varepsilon/2) \\
 p(\tau) &= p(\tau + \varepsilon/2) + \varepsilon \Delta \mathcal{L}(\boldsymbol{\theta}(\tau + \varepsilon))/2.
 \end{aligned}$$

The parameter τ is a placeholder to explain the proposal as a path. This approach does improve the acceptance rates for sampling posterior draws for the Ising model parameters. However, it often got stuck in flat areas of the likelihood.

The Riemann Manifold Adjusted Hamiltonian Monte Carlo (RMAHMC) method used in this work is simply an extension of the traditional HMC sampling using principles from the MALA algorithm to incorporate the geometry of a Riemann manifold (Girolami and Calderhead 2011). This adaptation allows for efficient sampling of high-dimensional parameter spaces, making it particularly useful in Bayesian statistics. In its simplest form it uses the metric tensor $G(\cdot)$ as the prior variance of the momentum parameters, $p \sim N(0, G(\boldsymbol{\theta}))$, instead of the mass matrix \mathbb{M} . This does complicate the sampling because the distribution for the momentum parameters is now a function of the parameters.

This combination of MALA and HMC sampling was much more consistent than either on its own and led to good sampling, but it often took several millions of draws to converge. To speed up the algorithm, we adopted a hybrid model with adaptive Metropolis-Hastings. Essentially, the algorithm alternated between a RMAHMC draw and a AMH draw. The RMAHMC draws have a more controllable acceptance depending on ε but moves very slowly and sometimes even in the wrong direction in certain parts of the likelihood while searching for the correct posterior space for convergence. The AMH draws can make larger jumps which are almost always rejected, but in many cases have helped find posterior convergence in a fraction of the samples. Algorithm 1 details the full method.

Algorithm 1 Hybrid RMAHMC-AMH Sampler

- 1: **Input:** Initial values $\boldsymbol{\theta}_0$, total number of samples N , step sizes ε
- 2: **Output:** Samples $\boldsymbol{\theta}_1, \dots, \boldsymbol{\theta}_N$
- 3: **Initialize:** Set $\boldsymbol{\theta} \leftarrow \boldsymbol{\theta}_0$
- 4: **for** $i = 1$ to N **do**
- 5: **if** i is odd **then**
- 6: **Run RMAHMC Draw (draw)**
- 7: Compute the log-gradient of the likelihood, $\Delta\mathcal{L}(\boldsymbol{\theta})$,
- 8: Compute the Hessian $G(\boldsymbol{\theta})$
- 9: Sample momentum $p \sim N(0, G(\boldsymbol{\theta}))$
- 10: Perform leapfrog steps with step size ε to propose $\boldsymbol{\theta}^*$
- 11: Compute acceptance rate $A(\boldsymbol{\theta}, \boldsymbol{\theta}^*)$
- 12: Accept or reject $\boldsymbol{\theta}^*$ based on A
- 13: **else**
- 14: **Run Adaptive Metropolis-Hastings Draw (draw2)**
- 15: Compute covariance of prior draws, C
- 16: Generate proposal $\boldsymbol{\theta}^*$ from a random walk, $N(\boldsymbol{\theta}_{i-1}, \frac{1}{3}C)$
- 17: Compute acceptance rate $A(\boldsymbol{\theta}, \boldsymbol{\theta}^*)$
- 18: Accept or reject $\boldsymbol{\theta}^*$ based on A
- 19: **end if**
- 20: Save the sample $\boldsymbol{\theta}$
- 21: **end for**

In order to provide more detail regarding $\Delta\mathcal{L}(\boldsymbol{\theta})$ and $G(\boldsymbol{\theta})$ in Algorithm 1, let μ_k be the k -th theoretical moment of the model distribution as functions of h , J , and K . Then the log-gradient of the likelihood, $\Delta\mathcal{L}(\boldsymbol{\theta})$, is calculated as follows:

$$\Delta\mathcal{L} = \begin{bmatrix} \frac{N}{3} \sum_{i=1}^n (m_i^3 - \mu_3) \\ \frac{N}{2} \sum_{i=1}^n (m_i^2 - \mu_2) \\ N \sum_{i=1}^n (m_i - \mu_1) \end{bmatrix}$$

and the Hessian matrix, $G(\boldsymbol{\theta})$, is calculated as follows:

$$G = N^2 \begin{bmatrix} \mu_2 - \mu_1^2 & \frac{1}{2}(\mu_3 - \mu_2\mu_1) & \frac{1}{3}(\mu_4 - \mu_1\mu_3) \\ \frac{1}{2}(\mu_3 - \mu_2\mu_1) & \frac{1}{4}(\mu_4 - \mu_2^2) & \frac{1}{6}(\mu_5 - \mu_2\mu_3) \\ \frac{1}{3}(\mu_4 - \mu_1\mu_3) & \frac{1}{6}(\mu_5 - \mu_2\mu_3) & \frac{1}{9}(\mu_6 - \mu_3^2) \end{bmatrix}.$$

The variance of the AMH steps was determined to be $\frac{1}{3}C$, where C is the covariance, from empirical observation for this specific model. It would likely need to be scaled differently for different likelihoods.

3.1 Computational Considerations

Despite the improved performance that the hybrid RMAHMC-AMH sampler exhibited, there are still a few of computational considerations that need to be addressed. For example, the geometry of the likelihood can make it so that the starting point for the Monte Carlo algorithm can result in poor behavior if not chosen intelligently. To aid in this process, we propose a simple grid search on the likelihood to determine a starting value. First, we define a coarse grid on the space of possible values for K , J , and h , evaluating the likelihood at each combination of these parameters. The algorithm begin at the parameter values associated with the largest likelihood. This procedure improves the probability of converging quickly.

An additional computational consideration is the numerical singularity of the Hessian matrix G . For certain values of θ the matrix can become numerically singular and cannot be used as a covariance to sample from, which is required for Algorithm 1. This is in fact one reason for the slow convergence of the RMAHMC algorithm without the adaptive steps because if bigger jumps are attempted, the probability of dealing with numerically singular matrix G increased. To address this, we reduce the off-diagonals by $(1 - \chi)100\%$ where χ is some small value, such as 0.0001. Surprisingly, even this small adjustment can affect mixing in a negative way. The issue of computational singularity does not affect the model when it has converged to the posterior, so to help with mixing and avoid computational errors, we start the algorithm with $\chi = 0.0001$ and then reduce to 0 after some burn-in.

4 Simulations Based on Challenging (K, J, h)

In this section we illustrate the performance of the algorithms detailed in Section 3 for some challenging estimation scenarios of the mean-field Ising model that have already been discussed in the literature (Contucci et al., 2023; Fedele et al., 2013; Decelle and Ricci-Tersenghi, 2016; Fedele and Vernia, 2017). This allows us to compare results here to those found in the literature. Further, we make an extension to critical point that were not studied in, Contucci et al. (2023) and discuss nonidentifiability in the parameter space. The specific cases we consider correspond to the inversion problem for values of $\theta = (K, J, h)$ where equation (10) of Appendix A has a unique maximum or multiple maximums. These scenarios are illustrated using three cases we refer to as the bimodal, unimodal, and nonidentifiable cases. In what follows, we display results using 5,000 MCMC samples for each of the three algorithms. We use the algorithm to find the starting values as discussed in Section 3.1, for most cases using a grid search with increments of 0.2. Two scenarios, $(0, 1.2, 0)$ and $(0, 1, 0)$, have true values that lie on the grid used for the starting value search. For these we arbitrarily use values that are not the truth as starting values. This also helps demonstrate the robustness of the hybrid method to starting values, as will be shown. Specifically we will see the following theme:

- Adaptive MCMC methods often get stuck in flat regions of the likelihood far from the truth, and when they do find the truth, correlations between parameters are high and mixing can be poor.
- Riemann manifold-adjusted Hamiltonian Monte Carlo eventually converges to the truth but it moves very slowly and will often takes hundreds of thousands of samples to achieve good results
- A hybrid method quickly identifies the true parameters and has good mixing once it

has found the truth.

The data is simulated in each case using $M = 1,000$ replicas of the configuration \mathbf{x} obtained for a fixed $N = 300$ vertex variables based on a fixed $\boldsymbol{\theta}$. These methods were tested at many numbers of spins with identical results. The number 300 was chosen as the added uncertainty in parameter estimation produces trace plots that more clearly illustrate the advantage of our computational approach. Lastly, we'd recommend running chains for more than 5,000 samples for reliable convergence, but to better illustrate the differences between the algorithms using trace plots 5,000 samples were employed.

4.1 Case 1: Bimodal Density

Multimodality in the distribution of $m_N(\mathbf{x})$, occurs when the likelihood (5) shows multiple peaks (Contucci et al., 2023; Fedele et al., 2013; Contucci et al., 2017; Nguyen et al., 2017; Fedele and Vernia, 2017). This phenomenon occurs when the equilibrium state of the system has multiple stable states which is manifest when equation (10) of the Appendix has multiple maxima, suggesting the presence of phase transition.

In such cases, addressing the inverse problem is challenging and typically approached locally for each stable state using clustering algorithms (Contucci et al., 2023; Decelle and Ricci-Tersenghi, 2016; Contucci et al., 2017; Rodriguez and Laio, 2014; Nguyen and Berg, 2012) or the spin-flip approach (Fedele and Vernia, 2017; Ito and Kohring, 1994). Clustering algorithms can be computationally expensive and the spin-flip approach works only when the model is globally spin-flip invariant for a given $\boldsymbol{\theta}$, (i.e., $P(\mathbf{x}; \boldsymbol{\theta}) = P(-\mathbf{x}; \boldsymbol{\theta})$). In the sequel, we will use the methods discussed in Section 3 for the recovery of two parameter scenarios: $K = h = 0, J = 1.2$, and $K = 1.67, J = 0.01, h = 0.1$ without having to resort to a two-step approach involving a preliminary clustering step.

4.1.1 Recovery of $(K, J, h) = (0, 1.2, 0)$ and $(K, J, h) = (1.67, 0.01, 0.1)$

The inversion problem for $(K, J, h) = (0, 1.2, 0)$ was solved using the spin-flip method (Fedele and Vernia, 2017) while that for $(K, J, h) = (1.67, 0.01, 0.1)$ was solved using a density clustering algorithm (Contucci et al., 2023), but based on 50 copies of M rather than a single copy that we consider here. Further, the point $(K, J, h) = (0, 1.2, 0)$ in the phase space is equivalent to the classical two-body interacting Ising model in the low temperature regime. The log-likelihood for these scenarios are shown in Figures 1(a) and 1(b). The irregular shapes of the log-likelihoods make constructing well behaved MCMC schemes challenging. To see this, Figure 2 display the MCMC chains for (K, J, h) corresponding to the AMH, RMAHMC, and RMAHMC-AMH algorithms respectively.

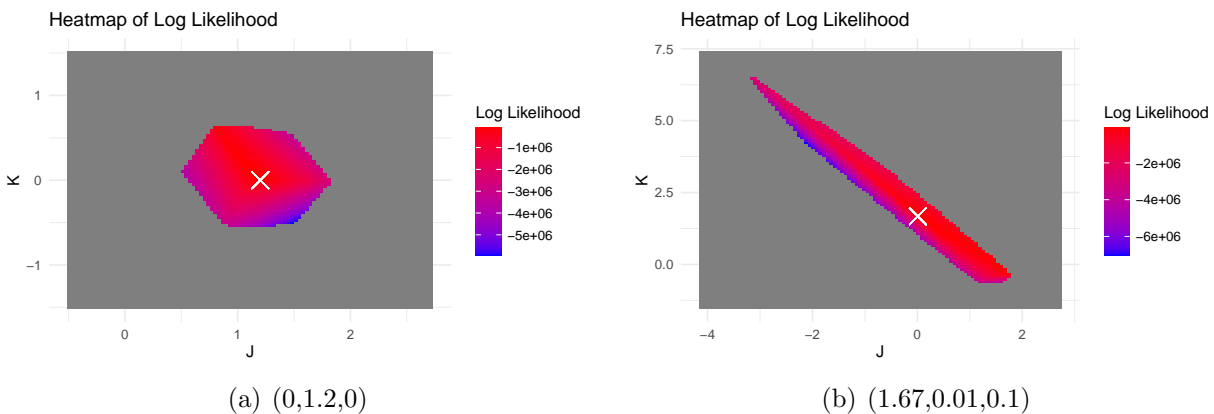


Figure 1: Plot (a) and (b) displays the log-likelihood as a function of K and J while keeping h fixed at 0. The white 'x' marker indicates the specific points (i.e., $(0, 1.2, 0)$ and $(1.67, 0.01, 0.1)$) in the parameter space we aim to recover. The gray phase corresponds to areas in the parameter space where the likelihood is numerically zero.

Focusing first on the left column of Figure 2 (the AMH algorithm), notice the poor mixing in both cases and the very slow convergence. For the middle column (i.e., the RMAHMC algorithm), convergence is also very slow requiring hundreds of thousands of MCMC iterations before convergence is met. The hybrid RMAHMC-AMH on the other hand converges very quickly (less than 2,000 iterations) and displays very good mixing. We

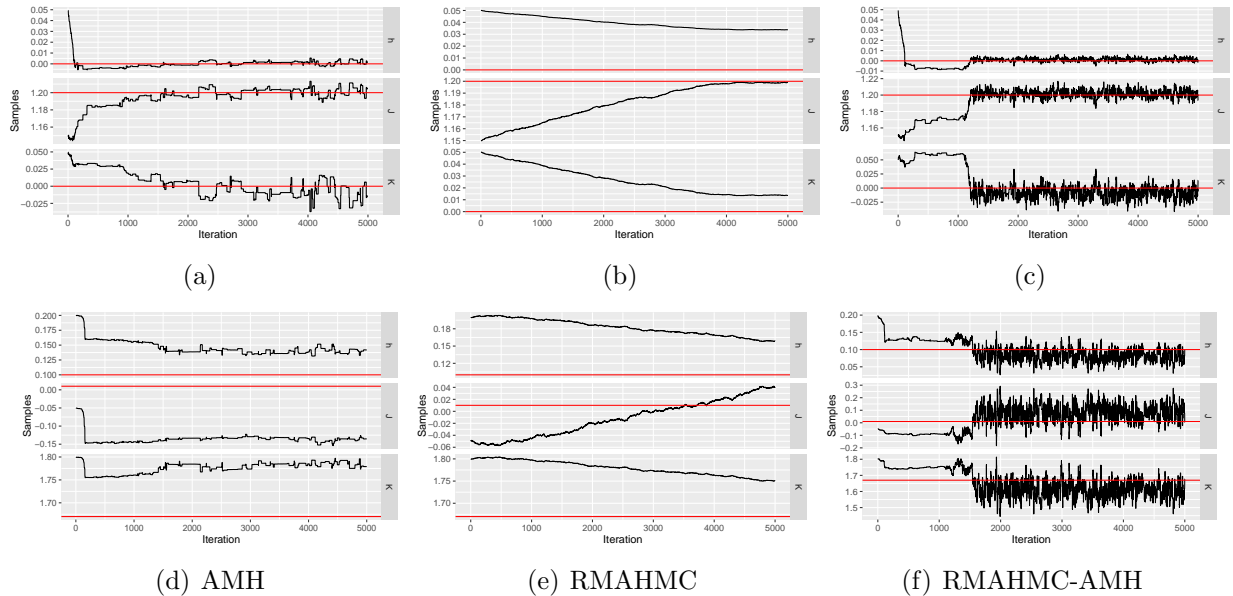


Figure 2: Trace plot of the MCMC samples collected from the posterior distribution of (K, J, h) based $N = 300$ and $M = 1000$ sampled configurations using $(K, J, h) = (0, 1.2, 0)$ (first row) and $(K, J, h) = (1.67, 0.01, 0.1)$ (second row).

discuss convergence diagnostics based on the Gelman-Rubin statistic in more detail for all scenarios and algorithms in Section 4.4.

We next construct the density of $m_N(\mathbf{x})$ in both scenarios using values for $\boldsymbol{\theta} = (K, J, h)$ estimated based on the MCMC samples collected. Figure 3(a) corresponds to the $(K, J, h) = (0, 1.2, 0)$ case, illustrating the two global stable states, where the red curve is obtained using the posterior mean of $\boldsymbol{\theta}$. For the $(K, J, h) = (1.67, 0.01, 0.1)$ case, notice that the equilibrium behavior of the system emerges to a metastable state with two peaks for smaller values of N (see Figure 3(b)).

4.2 Case 2: Unimodal Density

In this section we apply the MCMC algorithms described in Section 3 when the probability distribution of $m_N(\mathbf{x})$ is unimodal. We consider the two cases, $\boldsymbol{\theta} = (0.5, 0.3, 0.1)$ and a special one where the system is at its critical point $\boldsymbol{\theta} = (0, 1, 0)$ (Contucci et al., 2023). The

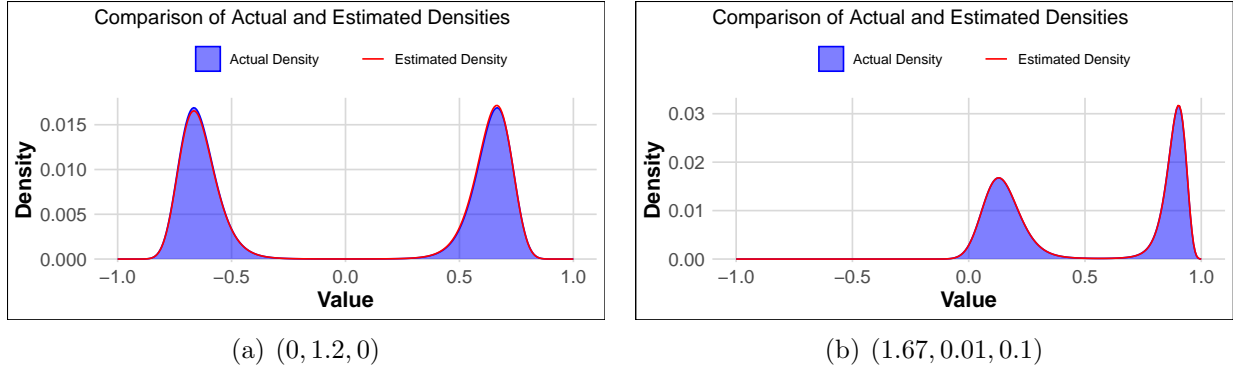


Figure 3: Boltzmann-Gibbs distribution of $m_N(\mathbf{x})$ at $N = 300$ with $M = 1000$ for the true and estimated parameters at (a) $(K, J, h) = (0, 1.2, 0)$ and (b) $(K, J, h) = (1.67, 0.01, 0.1)$. In (a), the peaks of the distribution are centered around two distinct and opposite values of $m_N(\mathbf{x})$ such that $Em_N(\mathbf{x}) = 0$. The two peaks corresponds to two global stable states of the system. The larger peak in (b) corresponds to a metastable state with probability approaching 0 as N increases. The red curve corresponds to the density plot estimated using MCMC samples collected based on the RMAHMC-AMH algorithm.

recovery of the triple $(0.5, 0.3, 0.1)$ is the easiest case, chosen to underscore the complexity of the second case, $(0, 1, 0)$. The inversion problem at the critical point $\boldsymbol{\theta} = (0, 1, 0)$ is crucial as it describes the point at which the system begins to transition from one stable state to another. This particular case was not addressed in Contucci et al. (2023), as at those values of the triple (K, J, h) , the susceptibility and third moment diverge to infinity and become analytically challenging. In this paper, we solve the inversion problem at $\boldsymbol{\theta} = (0, 1, 0)$ using the algorithms developed in Section 3.

4.2.1 Recovery of $(K, J, h) = (0.5, 0.3, 0.1)$ and $(K, J, h) = (0, 1, 0)$

The log-likelihood plot for the two scenarios $(0.5, 0.3, 0.1)$ and $(0, 1, 0)$ can be found as Figures 4(a) and 4(b) respectively. As in Section 4.1 the irregular shapes of these log-likelihoods makes it so that MCMC sampling of the posterior distribution of $\boldsymbol{\theta}$ is challenging.

Figure 5 displays the trace plots for the recovery of $\boldsymbol{\theta}$ under the the two scenarios using the MCMC algorithms described in Section 3. Focusing on the top row where $(K, J, h) = (0.5, 0.3, 0.1)$ the mixing from AMH and RMAHMC is better than those seen in Section

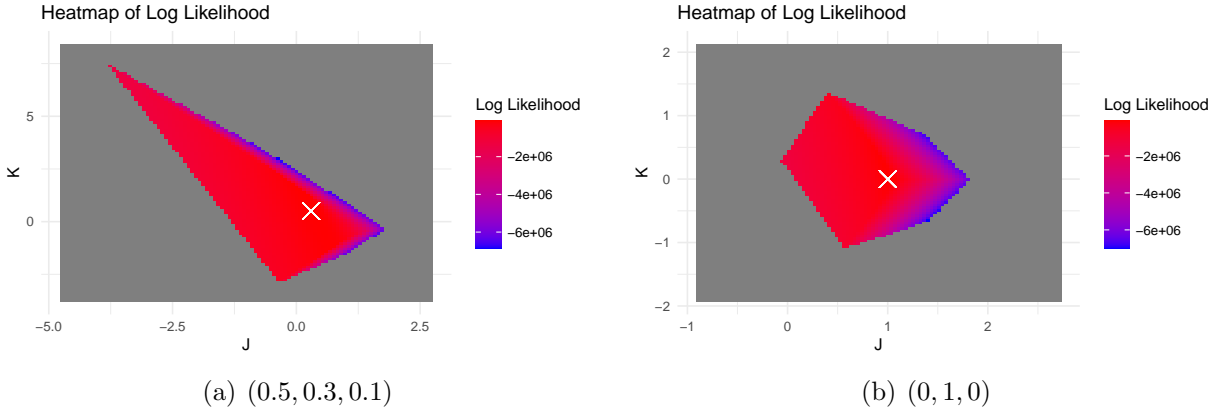


Figure 4: Plot (a) displays the log-likelihood as a function of K and J for fixed $h = 0.1$. Plot (b) displays the log-likelihood as a function of K and J while keeping h fixed at 0. The white ‘x’ marker indicates the point in the parameter space we aim to recover. The gray phase corresponds to areas in the parameter space where the likelihood is numerically zero and the red area depicts the flat regions of the likelihood function.

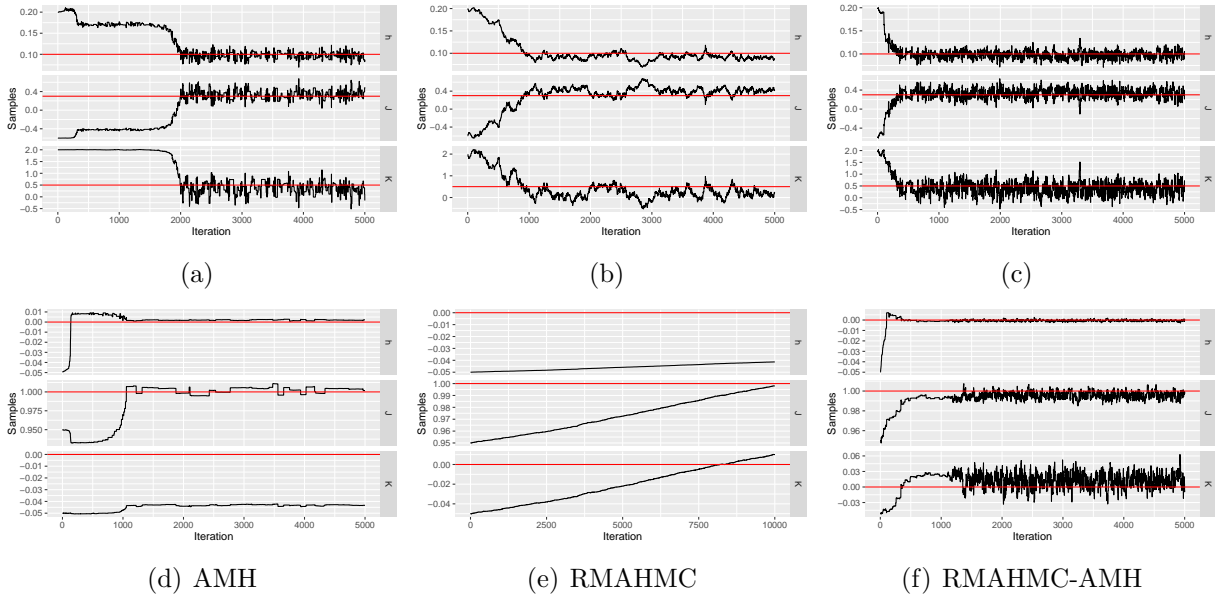


Figure 5: Trace plots associated with MCMC samples from the posterior distribution of (K, J, h) based on $N = 300$ and $M = 1000$ sampled configurations. The first row displays the three MCMC algorithms for the $(K, J, h) = (0.5, 0.3, 0.1)$ and the second row for $(K, J, h) = (0, 1, 0)$

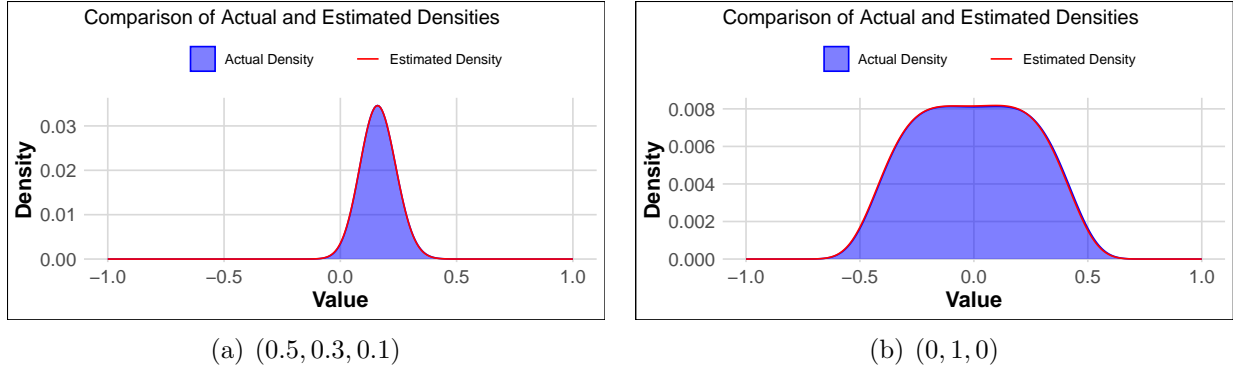


Figure 6: Boltzmann-Gibbs distribution of $m_N(\mathbf{x})$ at $N = 300$, with $M = 1000$ for the true and recovered parameters at (a) $\boldsymbol{\theta} = (0.5, 0.3, 0.1)$ and (b) the critical point $\boldsymbol{\theta} = (0, 1, 0)$. In (a), the peak of the distribution is centered around $Em_N(\mathbf{x})$ for fixed N and corresponds to a global stable state of the system while (b) has a flat mode, around $Em_N(\mathbf{x}) = 0$ as N increases.

4.1. However, the RMAHMC-AMH algorithm displays both better mixing and more rapid convergence. For the recovery of $(K, J, h) = (0, 1, 0)$, we see that, the AMH method gets stuck far from the truth for K while RMAHMC has slow convergence (see Figures 5(d) and 5(e)). Meanwhile the RMAHMC-AMH again displays good mixing and quick convergence (see Figure 5(f)). Next Figure 6 displays density estimates of $m_N(\mathbf{x})$ using the posterior mean of $\boldsymbol{\theta}$ based on MCMC iterates collected using RMAHMC-AMH. Notice that we are able to estimate the densities quite accurately even at the critical point $(K, J, h) = (0, 1, 0)$ (see Figure 6(b)).

4.3 Case 3: Nonidentifiable

The inversion problem for the last case we consider is particularly challenging, as it corresponds to a nonidentifiable scenario, making it the most difficult among the cases discussed. This complexity arises because numerous parameter combinations of K , J , and h yield nearly identical likelihoods. Perhaps making things even more challenging is that we were not able to determine concretely the subspace of $\boldsymbol{\theta}$'s support that resulted in a likelihood that was essentially flat. That said, this behavior does seem to be more prevalent when all three of

(K, J, h) are large with one such combination being $K = 0.5$, $J = 0.3$, and $h = 0.9$ which we consider now.

Focusing solely on the RMAHMC-AMH algorithm for this case (see Figure 8 of Appendix B for the trace plots of AMH and RMAHMC), Figure 7(b) shows that the algorithm converges to true values for (K, J, h) after about 2,000 MCMC iterations, but the width of the resulting credible intervals is significantly larger than those for the other cases considered previously. Figure 7(c) is the trace plot for the theoretical mean of the distribution (which we denote using b) which is a function of K , J , and h . Notice for b that MCMC chain is much less diffuse compared to K, J, h and still contains the truth. The behavior displayed in Figures 7(b) and 7(c) is typical of parameters that are poorly identified.

Figure 7(d) shows that the estimated density function matches the true density function well. This illustrates a case where specific combinations of parameters result in an accurate density fit, but individually seem to be estimated with large uncertainty. This too is a behavior that typically accompanies parameters that are poorly identified.

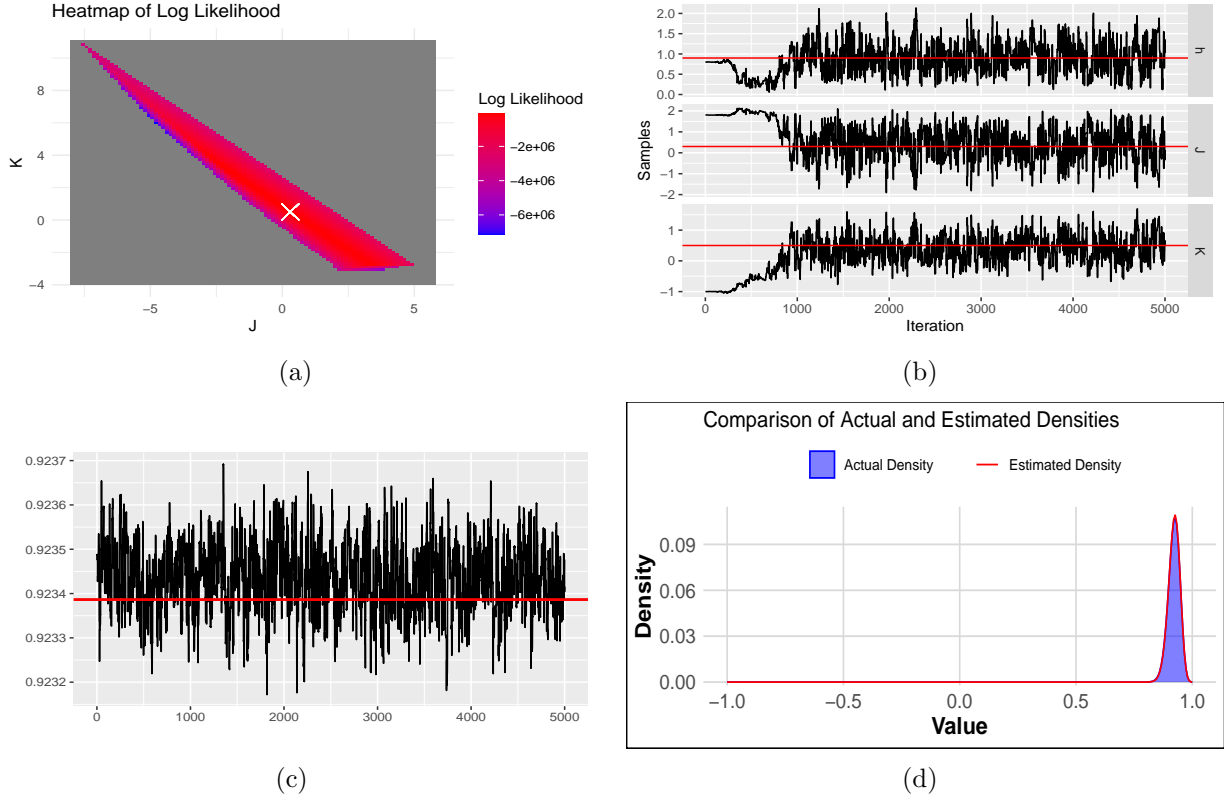


Figure 7: $K = 0.5, J = 0.3$ and $h = 0.9$. Plot (a) is the heatmap of the log-likelihood as a function of K and J for fixed $h = 0.9$. Plot (b) displays the trace plot of the hybrid RMHMC-AMH for parameter sampling from the posterior distribution at $N = 300$ and $M = 1,000$ sampled configurations. Plot (c) depicts the theoretical mean as a function of the recovered parameters and (d) is the associated density plot.

4.4 Convergence Measures

While the plots themselves are quite illustrative, it is helpful to see a more robust numeric measure of convergence. For this we use the Gelman-Rubin test statistic. The trace plots for all 5 scenarios have been shown for 5,000 samples. The small number of samples was motivated by the desire to highlight trends we were trying to illustrate. Now we run the sampler 100,000 times and show the Gelman-Rubin statistic for 5,000, 50,000, and 100,000 samples with burn-ins of 2,500, 40,000, and 90,000 respectively. The results are shown for only parameter K in Table 1 as results for J and h are very similar.

Table 1: Gelman Rubin Test Statistic for K

Scenario (K, J, h)	Sampler	Length of Run		
		5000	50000	100000
(0, 1.2, 0)	AMH	2.26	1.33	1.03
	RMAHMC	10.69	1.124	1.034
	Hybrid	1.009	1.0009	1.0009
(1.67, 0.01, 0.1)	AMH	1.18	1.04	1.001
	RMAHMC	2.02	1.007	1.05
	Hybrid	1.01	1.001	1.001
(0.5, 0.3, 0.1)	AMH	1.08	1.01	1.01
	RMAHMC	1.66	1.01	1.01
	Hybrid	1.008	1.002	1.001
(0, 1, 0)	AMH	8.44	7.55	1.96
	RMAHMC	20.98	1.07	1.006
	Hybrid	1.01	1.002	1.0007
(0.5, 0.3, 0.9)	AMH	4.75	1.79	2.63
	RMAHMC	1.005	1.007	1.003
	Hybrid	1.0001	1.0008	1.003

Gelman-Rubin statistic values that are very close to 1 suggest that convergence of an MCMC sampler to the correct target distribution has been met. It has been noted that even values above 1.1 can be cause for concern with regards to convergence (Gelman and Rubin, 1992). Table 1 is quite encouraging for all 3 samplers for more lengthy MCMC chains. However even with 100,000 samples, the AMH sampler struggles with the (0, 1, 0) and the (0.5, 0.3, 0.9) case. The hybrid method, as seen in these convergence results, is very consistent and attains convergence after a small number of MCMC iterations.

4.5 Simulation Study

To further explore the RMHMC-AMH's ability to recover parameters of the true data generating process, we conducted a small simulation study. This study consisted of generating 100 datasets based on the five sets of (K, J, h) values described in Section 4. For each data set

created, 95% credible intervals for (K, J, h) were estimated based on 2,500 MCMC iterates collected using the RMHMC-AMH algorithm and discarding the first 2,500 as burn-in. A total of 5,000 MCMC samples is sufficient because of the quick convergence and excellent mixing produced by the RMHMC-AMH algorithm. We then recorded the coverage (i.e., percent of intervals that contained the truth) and average credible interval width. The results are provided in Table 2. Notice that for all values of (K, J, h) the coverage is at or near the nominal 95% save for the nonidentifiable case where the coverage is 1, but at the cost of very wide intervals. The reason for this behavior was described in Section 4. The only other case whose coverage was further from 0.95 than expected was the parameter J corresponding to the point where phase transition begins. Rather than 0.95, the coverage was 0.9. Notice that for this case the intervals were much narrower than for the unimodal 1 case. Overall, this small simulation study illustrated the robust behavior of the RMHMC-AMH algorithm for difficult parameter settings corresponding to an Ising model with a three-body interaction.

Table 2: Results from the simulation study for each of the θ vectors considered.

case	$\theta = (K, J, h)$	coverage	width
Bimodal 1	(1.67, 0.01, 0.10)	(0.95, 0.96, 0.97)	(0.224, 0.284, 0.077)
Bimodal 2	(0.00, 1.20, 0.00)	(0.98, 0.94, 0.98)	(0.042, 0.019, 0.006)
Unimodal 1	(0.50, 0.30, 0.10)	(0.97, 0.97, 0.99)	(0.990, 0.373, 0.033)
Unimodal 2	(0.00, 1.00, 0.00)	(0.96, 0.90, 0.95)	(0.055, 0.014, 0.003)
Nonidentifiable	(0.50, 0.30, 0.90)	(1.00, 1.00, 1.00)	(1.610, 2.813, 1.367)

5 Conclusion

In this paper, we solved an inverse problem for the classical mean-field Ising model with three-body interaction using the Bayesian paradigm. We employed methods from statistical mechanics to expand the normalization constant and develop a refined MCMC algorithm capable of accurately recovering the model parameters in situations usually considered chal-

lenging.

The likelihood function in the presence of three-body interaction was observed to have a distinct shape, which contributes to the inherent difficulty in parameter inference as compared to the classical Ising model with only two-body interaction. This suggests both analytical and numerical difficulties associated with parameter estimation for higher-order interacting models. We demonstrated the robustness of our algorithm (i.e., hybrid RMAHMC-AMH) via simulation studies and assessed convergence using the Gelman-Rubin statistics. Interestingly, we considered a peculiar scenario where the model parameters are deemed to be nonidentifiable and found that, even in such a case, our algorithm is able to estimate the true model density. The advances made in this work contributes novel insight into the literature of the Ising model and enables the possibility of applying this model and its advanced versions to data, as we extensively covered various scenarios.

In future work, we will address the problem of inferring community structure from graphs with higher-order interactions, specifically 3-cliques, which is of particular interest. In many scenarios focused on inferring community structure from a graph, a common motivation arises from constructing the graph by connecting individuals with similar behaviors. Consequently, a natural question emerges: Can this observed behavior serve as the data itself? In future work, we aim to investigate the prospect of recovering a community structure from independent copies of observed data using a stochastic block Ising model.

Appendix A Expansion of the Partition Function

This section contains the proof of Lemma 2.1 and also shows the existence of thermodynamic limit of the free-energy of the system.

Proof. Using that $P(\mathbf{x}; \boldsymbol{\theta})$ assigns equal probability to configurations having the same $m_N(\mathbf{x})$,

to obtain the number of such configurations becomes a combinatorial problem such that:

$$A_N(m) = \binom{N}{\frac{N(1+m)}{2}} = \frac{N!}{\left(\frac{N(1+m)}{2}\right)! \left(\frac{N(1-m)}{2}\right)!} \quad (7)$$

where $\frac{N(1+m)}{2}$ corresponds to the number of vertices with +1 orientation and $\frac{N(1-m)}{2}$ the number of vertices with -1 orientation. To obtain the lower bound of A_N , we employ Stirling's approximation of a factorial, $N! = N^N e^{-N} \sqrt{2\pi N} (1 + \mathcal{O}(N^{-1}))$, such that:

$$\begin{aligned} \binom{N}{\frac{N(1+m)}{2}} &= \frac{N!}{\frac{N(1+m)}{2}! \frac{N(1-m)}{2}!} = \sqrt{\frac{2}{\pi N(1-m^2)}} \\ &\cdot \exp\left(\underbrace{-N \left(\frac{1-m}{2} \ln\left(\frac{1-m}{2}\right) + \frac{1+m}{2} \ln\left(\frac{1+m}{2}\right)\right)}_{=I(m)}\right) \cdot (1 + \mathcal{O}(N^{-1})). \end{aligned}$$

The lower bound follows from the last equality.

Let's suppose that the variables x_i are independent such that $\mathbb{P}(x_i = +1) = \mathbb{P}(x_i = -1) = 1/2$. Then the upper bound of A_N can be obtained using tail estimation. Observe that, if x_i are independent for all $i = 1, \dots, N$, then all configuration of Ω , has equal probability of having an empirical mean m and thus,

$$A_N = 2^N \mathbb{P}(m_N(\mathbf{x}) = m) \leq 2^N \mathbb{P}\left(\sum_{i=1}^N x_i \geq Nm\right).$$

The last inequality above follows from the the definition of $m_N(\mathbf{x})$ and leads to a tail estimation, since x_i is a random variable assumed to be independent and distributed with equal probability i.e., $\rho = 1/2(\delta_{y-1} + \delta_{y+1})$ for $y \in \{1, -1\}$. Therefore, for any $\lambda > 0$,

$$\begin{aligned} \mathbb{P}\left(\sum_{i=1}^N x_i \geq Nm\right) &\leq \exp(-\lambda m N) \prod_{i=1}^N \mathbb{E}_\rho \exp(\lambda \sigma_i) \\ &= \exp(N(-\lambda m + \ln \cosh(\lambda))). \end{aligned} \quad (8)$$

Optimizing over all λ , we obtain that

$$\lambda = \operatorname{arctanh}(m) = \frac{1}{2} \ln \left(\frac{1+m}{1-m} \right)$$

and it follows that since $1/\cosh^2(y) = 1 - \tanh^2(y)$, then $\ln \cosh(\lambda) = -1/2 \ln(1 - m^2)$.

Substituting this observation into (8), we have that

$$A_N \leq \exp(-NI(m)).$$

$I(m)$ is the entropy, also referred to as rate function, associated with m . It represents the logarithm of the number of ways m can be realized from different \mathbf{x} configurations and serves as a measure of the disorder in the system for a given configuration \mathbf{x} . It is worth noting that the results derived in this context can be used to obtain a large deviation approximation of the likelihood (1) for the event $m_N(\sigma) = m$. However, for our analysis, we rely on the precise form of $A_N(m)$. □

Notice that the sum over the spectrum S_m of the partition function has $N + 1$ terms. Since we are interested in behavior of the system in the exponential scale, we keep only the dominating terms (Talagrand, 2003; Friedli and Velenik, 2017);

$$\frac{1}{L} \frac{1}{\sqrt{N}} \exp \left(N \left(\max_{m \in [-1,1]} f(m) \right) \right) \leq Z \leq (N + 1) \exp \left(N \left(\max_{m \in [-1,1]} f(m) \right) \right) \quad (9)$$

where,

$$f(m) = \frac{K}{3} m^3 + \frac{J}{2} m^2 + hm - I(m).$$

Now with the expanded form of the normalizing constant, we can show the existence of thermodynamic limit of the pressure per particle governing the asymptotic behavior of the system. We define the pressure per particle which equals the free-energy up to a multiplica-

tive constant as:

$$p_N = \frac{1}{N} \ln Z$$

and it's thermodynamic limit $p = \lim_{N \rightarrow \infty} p_N$ is obtained as follows:

$$-\frac{1}{N} \left(\ln L + \frac{1}{2} \ln N \right) + \max_{m \in [-1,1]} f(m) \leq p_N \leq \frac{1}{N} \ln(N+1) + \max_{m \in [-1,1]} f(m)$$

and

$$p = \lim_{N \rightarrow \infty} p_N = \max_{m \in [-1,1]} f(m).$$

Hence

$$p = \max_{m \in [-1,1]} \left\{ \frac{K}{3} m^3 + \frac{J}{2} m^2 + hm - I(m) \right\}. \quad (10)$$

It is obvious from (10) that the maximizers satisfy the following consistency equation:

$$m = \tanh(Km^2 + Jm + h)$$

and equals (6) for a given $m_N(\mathbf{x})$ if $P(m_N(\mathbf{x}))$ is unimodal and N is large enough.

Appendix B AMH and RMAHMC: Nonidentifiable case

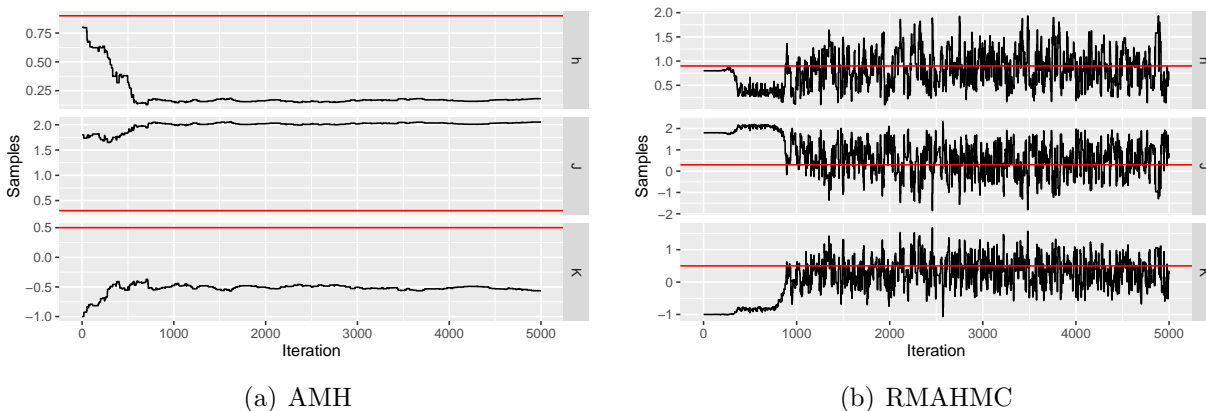


Figure 8: Trace plot associated to the AMH and RMAHMC algorithm for the recovery of $(K, J, h) = (0.5, 0.3, 0.9)$ with $N = 300$ and $M = 1000$ sampled configurations.

References

- Alvarez-Rodriguez, U., Battiston, F., de Arruda, G. F., Moreno, Y., Perc, M., and Latora, V. (2021), “Evolutionary dynamics of higher-order interactions in social networks,” *Nature human behaviour*, 5, 586–595, URL <http://dx.doi.org/10.1038/s41562-020-01024-1>.
- Aurell, E. and Ekeberg, M. (2012), “Inverse Ising Inference Using All the Data,” *Phys. Rev. Lett.*, 108, 090201, URL <https://link.aps.org/doi/10.1103/PhysRevLett.108.090201>.
- Barra, A., Contucci, P., Sandell, R., and Vernia, C. (2014), “An analysis of a large dataset on immigrant integration in Spain. The statistical mechanics perspective on social action,” *Scientific reports*, 4, 4174.
- Battiston, F., Amico, E., Barrat, A., Bianconi, G., Ferraz de Arruda, G., Franceschiello, B., Iacopini, I., Kéfi, S., Latora, V., Moreno, Y., Murray, M. M., Peixoto, T. P., Vaccarino, F., and Petri, G. (2021), “The physics of higher-order interactions in complex systems,” *Nature physics*, 17, 1093–1098, URL <http://dx.doi.org/10.1038/s41567-021-01371-4>.
- Baxter, R. J. (2016), *Exactly solved models in statistical mechanics*, Elsevier.
- Benson, A. R., Abebe, R., Schaub, M. T., Jadbabaie, A., and Kleinberg, J. (2018), “Simplicial closure and higherorder link prediction,” *Proc. Natl Acad. Sci. USA*, 115, E11221–E11230, URL <http://dx.doi.org/10.1073/pnas.1800683115>.

- Bhattacharya, B. B. and Mukherjee, S. (2018), “Inference in Ising models,” *Bernoulli: official journal of the Bernoulli Society for Mathematical Statistics and Probability*, 24, 493–525, URL <http://dx.doi.org/10.3150/16-bej886>.
- Borysov, S. S., Roudi, Y., and Balatsky, A. V. (2015), “US stock market interaction network as learned by the Boltzmann machine,” *The European Physical Journal B*, 88, 1–14.
- Brock, W. A. and Durlauf, S. N. (2001), “Discrete choice with social interactions,” *The Review of Economic Studies*, 68, 235–260.
- Burger, J., Isvoranu, A.-M., Lunansky, G., Haslbeck, J., Epskamp, S., Hoekstra, R. H., Fried, E. I., Borsboom, D., and Blanken, T. F. (2022), “Reporting standards for psychological network analyses in cross-sectional data.” *Psychological methods*.
- Burioni, R., Contucci, P., Fedele, M., Vernia, C., and Vezzani, A. (2015), “Enhancing participation to health screening campaigns by group interactions,” *Scientific Reports*, 5, 9904.
- Bury, T. (2013), “Market structure explained by pairwise interactions,” *Physica A: Statistical Mechanics and its Applications*, 392, 1375–1385.
- Chatterjee, S. (2007), “Estimation in spin glasses: A first step,” *Annals of statistics*, 35, 1931–1946, URL <http://dx.doi.org/10.1214/009053607000000109>.
- Contucci, P., Kertész, J., and Osabutey, G. (2022), “Human-AI ecosystem with abrupt changes as a function of the composition,” *PloS one*, 17, e0267310, URL <http://dx.doi.org/10.1371/journal.pone.0267310>.
- Contucci, P., Luzi, R., and Vernia, C. (2017), “Inverse problem for the mean-field monomer-dimer model with attractive interaction,” *Journal of physics. A, Mathematical and theoretical*, 50, 205002, URL <http://dx.doi.org/10.1088/1751-8121/aa69ef>.
- Contucci, P., Mingione, E., and Osabutey, G. (2024), “Limit theorems for the cubic mean-field Ising model,” in *Annales Henri Poincaré*, Springer.
- Contucci, P., Osabutey, G., and Vernia, C. (2023), “Inverse problem beyond two-body interaction: The cubic mean-field Ising model,” *Phys. Rev. E*, 107, 054124, URL <https://link.aps.org/doi/10.1103/PhysRevE.107.054124>.
- Contucci, P. and Vernia, C. (2020), “On a statistical mechanics approach to some problems of the social sciences,” *Frontiers in Physics*, 8, 585383.
- Decelle, A. and Ricci-Tersenghi, F. (2016), “Solving the inverse Ising problem by mean-field methods in a clustered phase space with many states,” *Physical review. E*, 94, 012112, URL <http://dx.doi.org/10.1103/PhysRevE.94.012112>.

- Durlauf, S. N. (1999), “How can statistical mechanics contribute to social science?” *Proceedings of the national academy of sciences*, 96, 10582–10584.
- Fedele, M. and Vernia, C. (2017), “Inverse problem for multispecies ferromagneticlike mean-field models in phase space with many states,” *Physical review. E*, 96, 042135, URL <http://dx.doi.org/10.1103/PhysRevE.96.042135>.
- Fedele, M., Vernia, C., and Contucci, P. (2013), “Inverse problem robustness for multispecies mean-field spin models,” *J. of Phys. A: Math. and Theo.*, 46, 065001, URL <https://doi.org/10.1088/1751-8113/46/6/065001>.
- Friedli, S. and Velenik, Y. (2017), *Statistical Mechanics of Lattice Systems: A Concrete Mathematical Introduction*, Cambridge University Press.
- Gallo, I., Barra, A., and Contucci, P. (2009), “Parameter evaluation of a simple mean-field model of social interaction,” *Mathematical Models and Methods in Applied Sciences*, 19, 1427–1439.
- Gelman, A. and Rubin, D. B. (1992), “Inference from iterative simulation using multiple sequences,” *Statistical science*, 7, 457–472.
- Geman, S. and Graffigne, C. (1986), “Markov random field image models and their applications to computer vision,” in *Proceedings of the International Congress of Mathematicians*.
- Girolami, M. and Calderhead, B. (2011), “Riemann manifold Langevin and Hamiltonian Monte Carlo methods: Riemann Manifold Langevin and Hamiltonian Monte Carlo Methods,” *Journal of the Royal Statistical Society. Series B, Statistical methodology*, 73, 123–214, URL <http://dx.doi.org/10.1111/j.1467-9868.2010.00765.x>.
- Goldstone, J. A. (2015), *The encyclopedia of political revolutions*, Routledge.
- Habeck, M. (2014), “Bayesian approach to inverse statistical mechanics,” *Phys. Rev. E*, 89, 052113, URL <https://link.aps.org/doi/10.1103/PhysRevE.89.052113>.
- Hamilton, W. L., Leskovec, J., and Jurafsky, D. (2016), “Cultural shift or linguistic drift? comparing two computational measures of semantic change,” in *Proceedings of the conference on empirical methods in natural language processing. Conference on empirical methods in natural language processing*, volume 2016, NIH Public Access.
- Inglehart, R. (2020), *Modernization and postmodernization: Cultural, economic, and political change in 43 societies*, Princeton university press.
- Ito, N. and Kohring, G. A. (1994), “Single-spin algorithms- Which are more efficient?” *Intl. J. Mod. Phys. C*, 05.
- Kappen, H. J. and Rodríguez, F. B. (1998), “Efficient learning in Boltzmann machines using linear response theory,” *Neural computation*, 10, 1137–1156, URL <http://dx.doi.org/10.1162/089976698300017386>.

- Kim, M., Bhattacharya, S., and Maiti, T. (2021), “Variational Bayes algorithm and posterior consistency of Ising model parameter estimation,” .
- Li, F. and Zhang, N. R. (2010), “Bayesian variable selection in structured high-dimensional covariate spaces with applications in genomics,” *Journal of the American Statistical Association*, 105, 1202–1214, URL <http://dx.doi.org/10.1198/jasa.2010.tm08177>.
- Marsman, M. and Rhemtulla, M. (2022), “Guest editors’ introduction to the special issue “network psychometrics in action”: Methodological innovations inspired by empirical problems,” *psychometrika*, 87, 1–11.
- McFadden, D. (2001), “Economic choices,” *American economic review*, 91, 351–378.
- Morcos, F., Pagnani, A., Lunt, B., Bertolino, A., Marks, D. S., Sander, C., Zecchina, R., Onuchic, J. N., Hwa, T., and Weigt, M. (2011), “Direct-coupling analysis of residue coevolution captures native contacts across many protein families,” *PNAS*, 108, E1293–E1301, URL <https://www.pnas.org/content/108/49/E1293>.
- Mézard, M. and Mora, T. (2009), “Constraint satisfaction problems and neural networks: A statistical physics perspective,” *Journal of physiology, Paris*, 103, 107–113, URL <http://dx.doi.org/10.1016/j.jphysparis.2009.05.013>.
- Nguyen, H. C. and Berg, J. (2012), “Mean-field theory for the inverse Ising problem at low temperatures,” *Physical review letters*, 109, 050602, URL <http://dx.doi.org/10.1103/PhysRevLett.109.050602>.
- Nguyen, H. C., Zecchina, R., and Berg, J. (2017), “Inverse statistical problems: from the inverse Ising problem to data science,” *Advances in physics*, 66, 197–261, URL <http://dx.doi.org/10.1080/00018732.2017.1341604>.
- Opoku, A. A., Osabutey, G., and Kwofie, C. (2019), “Parameter evaluation for a statistical mechanical model for binary choice with social interaction,” *Journal of probability and statistics*, 2019, 1–10, URL <http://dx.doi.org/10.1155/2019/3435626>.
- Osabutey, G., Opoku, A. A., and Gyamfi, S. (2020), “A statistical mechanics approach to the study of energy use behaviour,” *Journal of applied mathematics*, 2020, 1–14.
- Raue, A., Kreutz, C., Maiwald, T., Bachmann, J., Schilling, M., Klingmüller, U., and Timmer, J. (2009), “Structural and practical identifiability analysis of partially observed dynamical models by exploiting the profile likelihood,” *Bioinformatics (Oxford, England)*, 25, 1923–1929, URL <http://dx.doi.org/10.1093/bioinformatics/btp358>.
- Raue, A., Kreutz, C., Theis, F. J., and Timmer, J. (2013), “Joining forces of Bayesian and frequentist methodology: a study for inference in the presence of non-identifiability,” *Philosophical transactions. Series A, Mathematical, physical, and engineering sciences*, 371, 20110544, URL <http://dx.doi.org/10.1098/rsta.2011.0544>.

- Rodriguez, A. and Laio, A. (2014), “Machine learning. Clustering by fast search and find of density peaks,” *Science (New York, N.Y.)*, 344, 1492–1496, URL <http://dx.doi.org/10.1126/science.1242072>.
- Schneidman, E., Berry, M., Segev, R., and Bialek, W. (2006), “Weak pairwise correlations imply strongly correlated network states in a neural population,” *Nature*, 440, 1007–1012.
- Schug, A., Weigt, M., Onuchic, J. N., Hwa, T., and Szurmant, H. (2009), “High-resolution protein complexes from integrating genomic information with molecular simulation,” *PNAS*, 106, 22124–22129, URL <https://www.pnas.org/content/106/52/22124>.
- Skocpol, T. (1979), *States and social revolutions: A comparative analysis of France, Russia and China*, Cambridge University Press.
- Sohl-Dickstein, J., Battaglino, P. B., and DeWeese, M. R. (2011), “New Method for Parameter Estimation in Probabilistic Models: Minimum Probability Flow,” *Phys. Rev. Lett.*, 107, 220601, URL <https://link.aps.org/doi/10.1103/PhysRevLett.107.220601>.
- Subramanian, B. and Lebowitz, J. (1999), “The study of a three-body interaction Hamiltonian on a lattice,” *J. Phys. A: Math. Gen.*, 32.
- Talagrand, M. (2003), *Spin Glasses: A Challenge for Mathematicians-Cavity and mean-field Models*, Berlin: Springer.
- Weiss, P. (1907), “L’hypothèse du champ moléculaire et la propriété ferromagnétique,” *J. Phys. Theor. Appl.*, 6, 661–690.